Anomalous subsurface VLF electric field emissions related to Nepal earthquakes (M = 7.8, M = 7.3), and their generation and propagation mechanisms

Sarita Sharma[1], Raj Pal Singh[1,*], Birbal Singh[2] and Devbrat Pundhir[3]

[1]Department of Physics, GLA University, Chaumuhan, Mathura 281 406, India
[2]Department of Electronics and Communication, R.B.S. Engg. Tech. Campus, Bichpuri, Agra 283 105, India
[3]Department of Physics, R.B.S. Engg. Tech. Campus, Bichpuri, Agra 283 105, India

Measurements of amplitude of vertical components of very low frequency (VLF) electric field emissions have been in progress at Chaumuhan, Mathura (27.5°N, 77.68°E), Uttar Pradesh, India, at the frequency of 3.012 kHz using a borehole antenna since 24 March 2011. In the present study, we have statistically analysed the VLF data from 1 January to 31 July 2015 using the mean (m) and standard deviation (σ) around the mean ($m \pm 2\sigma$) criterion with respect to two major earthquakes (M = 7.8, 7.3) and their aftershocks that occurred on 25 April and 12 May 2015 in Khudi and Kodari regions of Nepal respectively. Results of the analysis show a spiky enhancement above the $m + 2\sigma$ line in the daily variation of the normalized VLF data, 7–14 days before the onset of main shocks of these earthquakes. These anomalous enhancements in the normalized values of amplitude are examined in light of various other possible causative sources such as magnetic storms, local lightning, solar flares and solar eclipse, rainfall, wind speed, temperature and pressure of the atmosphere. It was found that the VLF amplitude anomalies are not related to these sources. Further, we have developed a theoretical model for generation and propagation mechanisms of VLF emissions associated with the said earthquakes and their aftershocks by assuming an ensemble of elementary radiators randomly oriented and distributed in space and time in the preparation zones of these earthquakes. The computed electric field from the model is in good agreement with the observations.

Keywords: Attenuation, earthquakes, electric field, radiating dipole, VLF emissions.

EMPLOYING a ground-based receiver, Gokhberg *et al.*[1] first reported the anomalous increase in intensity of electromagnetic signals (f = 81 kHz) one hour before the onset of main shock (M = 7) in the central region of Japan. Since then, scientific efforts have started actively in this field and numerous electromagnetic phenomena have been observed in a wide band of frequencies ranging from ultra-low frequency (ULF; 0.01–10 Hz) to high frequency (HF; 3–30 MHz) employing ground and satellite-based techniques. A few notable among them are changes in intensity of direct current (DC)/ULF electric field emissions[2], subsurface very low frequency (VLF) electric field changes[3,4] and ionospheric electron density variation[5]. Laboratory experiments involving fracturing of rocks have confirmed the association of electromagnetic radiations with earthquakes[6]. A detailed account of the work done in this field can be found elsewhere[7,8].

Among the various ground-based techniques developed so far for monitoring the electromagnetic precursors of earthquakes, measurements of subsurface electric and magnetic field changes in VLF band (3–30 kHz) have attracted the attention of many workers in the recent past[3,4,9]. Using this technique, significant enhancement in the number of VLF pulses was observed by Fujinawa and Takahashi[10] in the frequency range 1–9 kHz two days before the Great Kurile earthquake (M = 8.1) that occurred on 4 October 1994. Anomalous amplitude enhancement in the vertical component of VLF electric field emissions at the frequency of 3 kHz was reported by Singh *et al.*[4] three hours prior to the occurrence of the Chamoli earthquakes of March/April 1999. Using a ground-buried sensor-type borehole antenna, Fujinawa *et al.*[3] recorded pulse-like signals having different waveforms six days before the Tohoku earthquake (M = 9.0) that occurred on 11 March 2011.

In the present study, we have statistically analysed the VLF data obtained from a borehole antenna from 1 January to 31 July 2015 with respect to two major earthquakes and their aftershocks that occurred on 25 April and 12 May 2015 in Khudi and Kodari regions of Nepal, and results of analysis are presented here. In addition, we have computed the strength of the electric field received at the observing station radiated by an ensemble (a group of radiating dipoles) of radiators (at the frequency of 3.012 kHz) present in the preparation zones of the Nepal

*For correspondence. (e-mail: rp.singh@gla.ac.in)

earthquakes, for explaining the observed experimental results. This study will provide a better understanding of the generation and propagation mechanisms of seismogenic emissions.

Experimental set-up

The routine observation of subsurface VLF electric field emissions at the frequency of 3.012 kHz has been in progress at Mathura (27.5°N, 77.68°E) observatory, Uttar Pradesh, India, since 24 March 2011, employing the experimental set-up shown in Figure 1. It consists of a borehole antenna which is a naked copper wire of length 120 m and 4 mm diameter, placed in a water-tight PVC pipe. Another electrode is placed 3 m down the earth, which provides ground terminal. This antenna is connected to a PC through an amplifier (gain ~26 dB), band-pass filter (peak frequency 3.012 kHz), notch filter (notch frequency 50 Hz) and A/D convertor. The experimental arrangement is similar to the one used at Agra station[4,11], except with three minor modifications which include: (i) a differential amplifier which eliminates common noises, (ii) a notch filter rejecting power-line radiations and (iii) digital recording of VLF signals that may provide information on their phase characteristics. The normalized electric field on the antenna is found to be around 6.83×10^{-3} mV/m at night-time in fair weather conditions. It is worthwhile to mention here that the experimental set-up has been deployed at GLA University, Chaumuhan, located 17 km west of Mathura city in a rural area where electrical and electromagnetic noises are very low. In addition, the peak frequency of band-pass filter is chosen to be 3.012 kHz as a trade-off between the spurious noises at lower frequencies produced due to power-line radiations and their harmonics and atmospherics, and increasing attenuation with frequency.

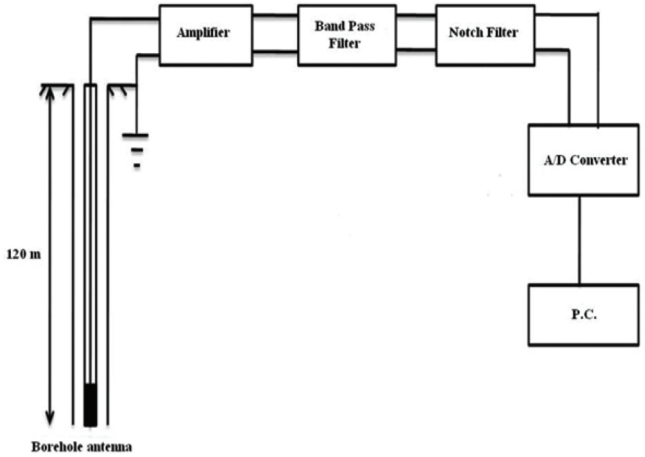

Figure 1. Experimental set-up at Mathura for monitoring vertical components of subsurface VLF electric field emissions.

Sources of earthquakes and parameters influencing the subsurface VLF electric field changes

Propagation of seismo-electromagnetic radiations is usually influenced by many parameters such as solar flares, solar eclipse, magnetic storms, local lightning, rainfall, wind speed, atmospheric pressure and temperature. During six months of data processing, we have examined the existence of these parameters and their influence on the propagation of vertical component of VLF electric field emissions. We found that a severe earthquake of magnitude $M = 7.8$ occurred 36 km east of Khudi, Nepal (28.33°N, 84.73°E) on 25 April 2015, which caused huge losses of lives and properties. This devastating earthquake was followed by another major shock of magnitude $M = 7.3$ in the Kodari region (27.7°N, 86.0°E) of Nepal on 12 May 2015. Many minor and a few major aftershocks ($M = 6.1$, 6.3, 6.6) also occurred on the same day after this major earthquake. Figure 2 shows the locations of the two major earthquakes in Nepal and the observing station at Mathura, India. Thick solid curves show the great circle path (GCP) distance of the epicenters of two major earthquakes of magnitudes 7.8 and 7.3 from the observing station which is 698 and 827 km respectively. Details of these two major Nepal earthquakes and their aftershocks are given in Table 1, which have

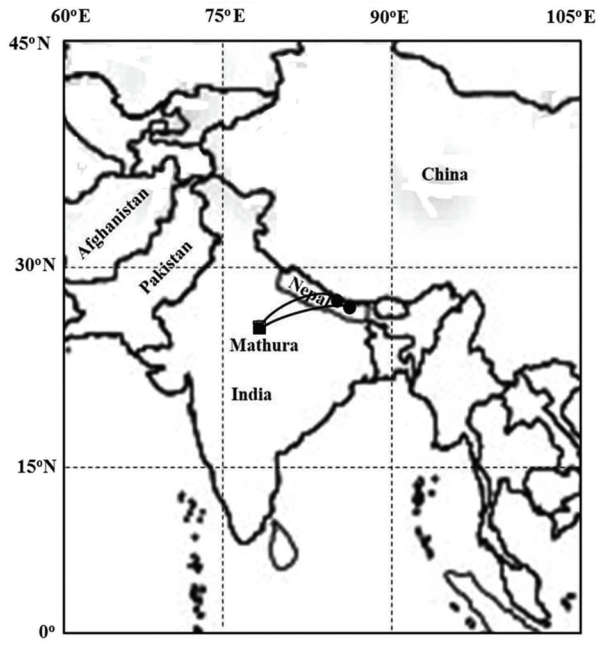

Figure 2. Map of India and its neighbouring countries showing the locations of Mathura observatory and Nepal earthquakes which occurred on 25 April and 12 May 2015 (solid square and solid circles respectively). Solid curved thick lines indicate the great circle paths between Mathura observatory and locations of earthquakes. However, the locations of major aftershocks of these earthquakes are not depicted in the map because all of them have occurred in the locations of these two major earthquakes.

Table 1. Details of two major Nepal earthquakes and their aftershocks considered in this study

Date of earthquake occurrence	Time of occurrence of earthquakes (LT)	Location of earthquakes		Magnitude of earthquakes (M)	Depth (km)	Distance of epicentre of earthquakes from Mathura station (km)
		Latitude	Longitude			
25/04/2015	11:41:25	28.23°N	84.73°E	7.8	8.22	698
25/04/2015	11:45:22	27.62°N	85.53°E	6.1	10	773
25/04/2015	12:15:21	28.22°N	84.82°E	6.6	10	706
12/05/2015	12:35:19	27.81°N	86.07°E	7.3	15	827
12/05/2015	13:06:54	27.62°N	86.16°E	6.3	15	835

been obtained from the United States Geological Survey (USGS) through their website (http://neic.usgs.gov).

In order to examine the effect of magnetic storms on VLF data recorded at observing station, Mathura magnetic storm data were procured from the World Data Center, Kyoto, Japan (website: http://swdcdb.kugi.kyotse.ac.jp). The solar eclipse data were obtained from the National Aeronautics and Space Administration (NASA; www.nasa.gov/eclipse) and the solar flare data were obtained from the website www.spaceweather.com. The local lightning and rainfall data were obtained from the website www.woundergrund.com and finally, the data for meteorological parameters like wind speed, temperature and pressure of the atmosphere corresponding to the period of observations were obtained from the website https://power.larc.nasa.gov/data-access-viewer.

Method of observation and data processing

As mentioned earlier, digital recording of vertical component of subsurface VLF electric field emissions was started at Chaumuhan, Mathura on 24 March 2011, employing the experimental set-up of Figure 1. The reason for monitoring only this component is that in long-distance propagation, horizontal components are attenuated. Other workers have also monitored the same[3]. The routine data were logged at the rate of 1 sample/s round the clock and bulk of the data recorded on each day was averaged out. In order to minimize the effect of local building noises and power-line radiations, only the night-time data (19:00–05:00 h LT, LT = UT + 5.5 h) of each day were considered in the present analysis. During night-time, various electrical and electromagnetic devices such as electric motor, table lamp, computer, monitor, etc. and the power lines connecting them are usually in switch-off mode and hence do not generate their harmonics; hence voltage induced in the antenna remains unaltered. Other workers have also used the night-time data in their studies[12].

Several reports indicating that precursory time ranges from a few days to a few months are available[7,8]. Keeping this in view, we considered six months data and normalized them using the relation $\mathrm{DATA}^* = \frac{\mathrm{DATA} - \overline{\mathrm{DATA}}}{\sigma}$ given by Muto *et al.*[13], where $\overline{\mathrm{DATA}}$ is the monthly mean of night-time VLF data and σ is the standard deviation. Such type of normalization eliminates seasonal effects on the data, if any. The normalized data were then analysed statistically considering the mean and standard deviation around the mean approach.

Results

Diurnal variation of subsurface VLF electric field and identification of amplitude anomalies

Figure 3 *a* and *b* shows the results of data analysis. In Figure 3 *a* daily variations of normalized amplitude of subsurface VLF electric field changes for the period from January to April 2015 are shown, whereas the same is shown in Figure 3 *b* for the period from May to July 2015. The data for February 2015 were not available due to power failure, and hence are not shown in Figure 3 *a*. The mean (m) and standard deviation around the mean ($m \pm 2\sigma$) criteria have been used for high degree of confidence[14]. Similar approach has also been adopted by other workers in VLF studies related to seismic activities[14]. The variation of magnetic storm parameter $\sum Kp$ (solid bars) and the occurrence of local lightning (solid stars) during each month are also shown in the figure. The open stars show the days of occurrence of earthquakes and their aftershocks.

From the top two panels shown for January and March in Figure 3 *a*, it is evident that the normalized electric field varies almost along the monthly mean value during all the days for both months. However, in the bottom panel which corresponds to April, the amplitude of electric field varies normally along the monthly mean all the days, except on 11 April 2015, when an anomalous enhancement above $m + 2\sigma$ line occurred. Figure 3 *b* shows similar variations of electric field. In the top panel of this figure, a spiky enhancement in amplitude of VLF data can be observed on 5 May, which then repeats on 29 June and 6, 10 and 23 July 2015. An interesting result seen in these figures is that all the anomalous enhancements are followed by major or minor earthquakes.

Table 2 shows the precursory days of these anomalies from the respective days of earthquakes. Figure 4 shows these results graphically. It is clear that precursory time

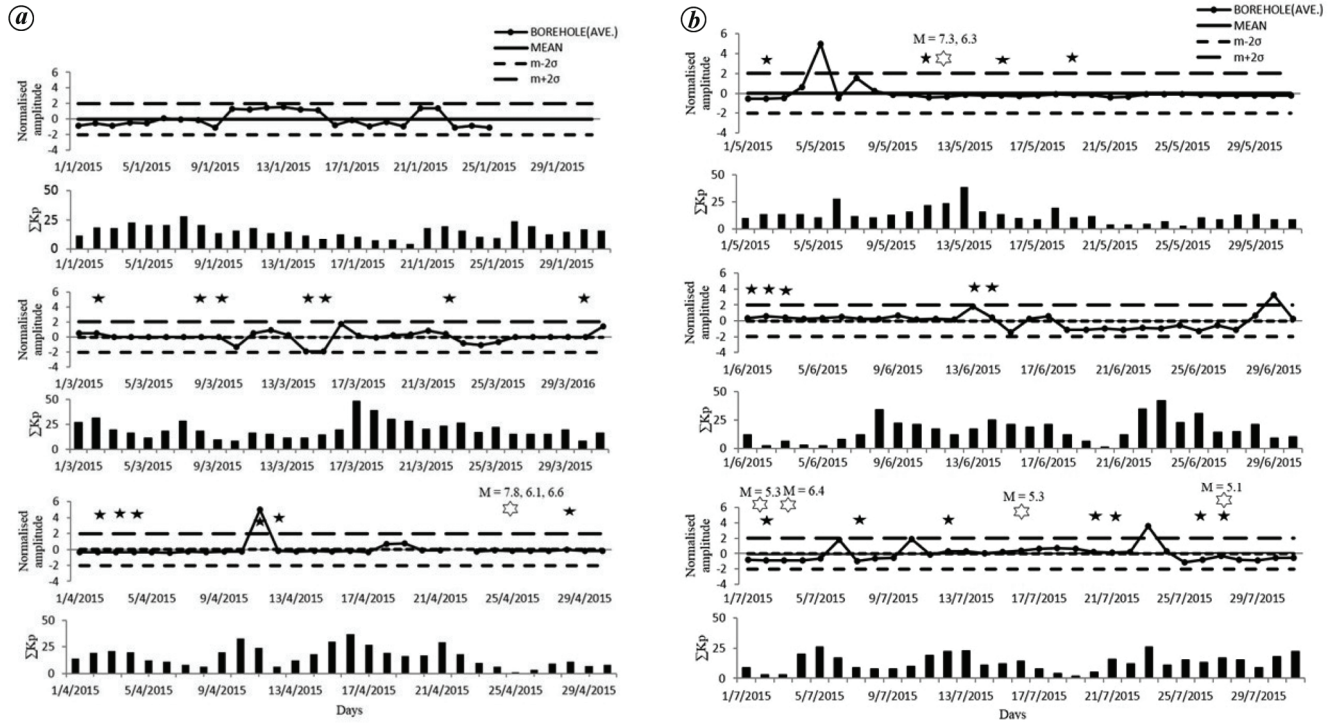

Figure 3. ***a***, Daily variation of vertical component of subsurface VLF electric field emissions (shown by solid curved line with dots) for the period from January to July 2015. The horizontal solid straight line indicates monthly mean (m), while dashed lines show standard deviation around the mean ($m \pm 2\sigma$). Open stars show the dates and magnitudes of the earthquakes and their aftershocks, while solid stars show the days of occurrence of lightning activity as observed at Delhi about 150 km north of Mathura. (Bottom panel) Daily variation of $\sum Kp$ for the same period shown by solid bars. ***b***, Same as (***a***), but here the variations for both the subsurface VLF electric field emission and $\sum Kp$ data are considered for the period from May to July 2015.

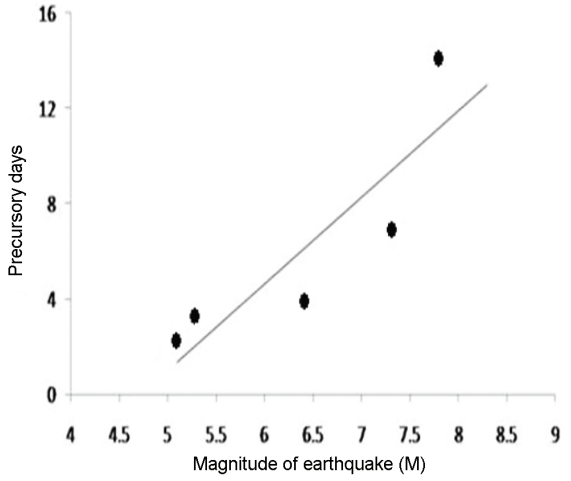

Figure 4. Variation of precursory days with magnitude of earthquakes corresponding to which amplitude anomalies are observed at Mathura observatory in borehole antenna.

of earthquakes increases with increase in their magnitude. Similar results have also been reported in Pundhir *et al.*[15]. This result is also supported by the relation between magnitude (M) of an earthquake and precursory time (T); $\log T = 0.76M - 1.83$, as proposed by Rikitake[16] taking different types of precursors into account.

The anomalies in Figure 3 *a* and *b* are attributed to the various earthquakes shown in it. We have not examined the influence of magnetic storm and lightning which are also shown in the figure. In the following, we examine the effect of these parameters along with some of the meteorological parameters mentioned earlier which may also influence the diurnal variation of electric field.

Influence of other parameters on the amplitude anomalies

From Figure 3 *a* and *b*, we find that the magnetic storms have not influenced the anomalous enhancement in normalized VLF amplitude variation because: (i) some of them have occurred after the anomalies, (ii) the days of occurrence do not correspond to the days of anomalous amplitude enhancement, and (iii) other storms are of low strength ($\sum Kp < 30$). In order to explain this one may be reminded that the effect of magnetic storms is high at high latitudes, moderate at mid-latitudes, low at low latitudes, and sometimes disappears at low and equatorial latitudes on account of weakening of the effect of ring current on reaching there[17].

From Figure 3 it is clear that none of the lightning occurrences could affect the daily variation of electric field during the whole period of observations, except on

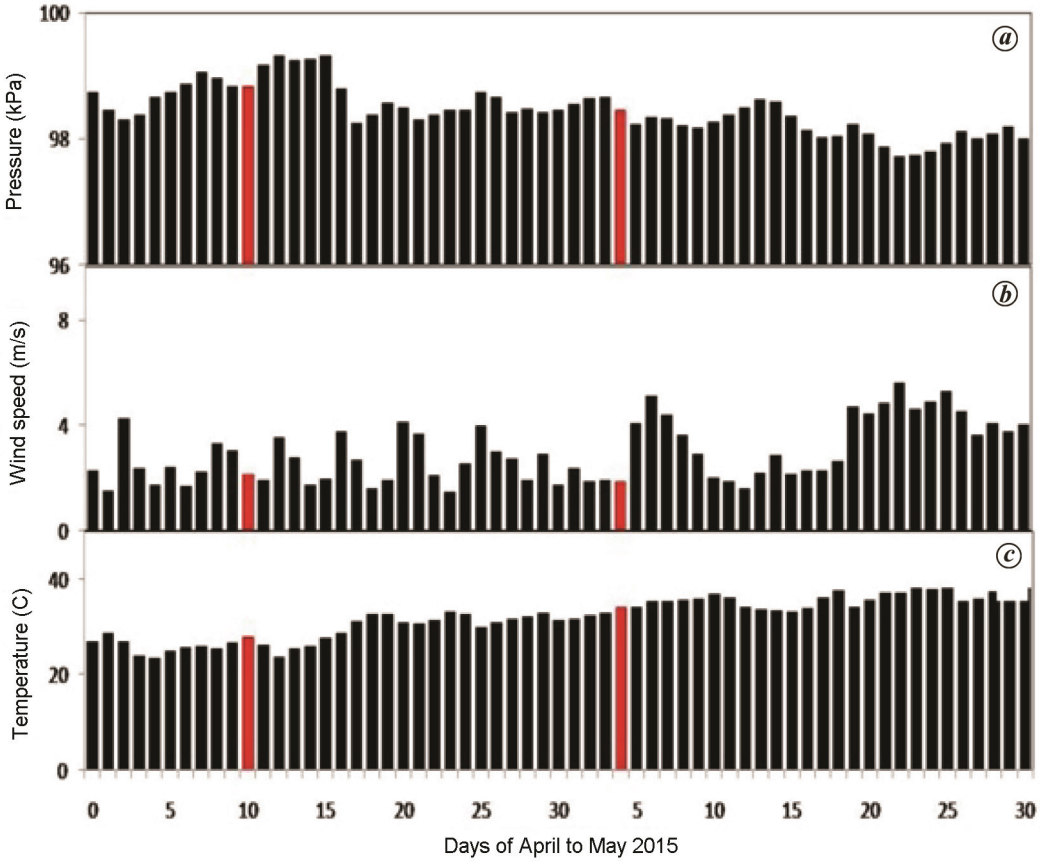

Figure 5. Daily variations of wind speed, temperature and pressure from 1 April to 31 May 2015 shown by histograms. ***a***, Variation of wind speed (m/s). ***b***, ***c***, Variation of temperature (°C) and pressure of the atmosphere (kPa) respectively. The histograms marked by 'red' show wind speed, temperature and pressure values of the atmosphere on the days of the earthquakes.

Table 2. Magnitude of earthquakes for which VLF amplitude anomalies are observed as a precursor in borehole antenna

Magnitude of earthquakes (*M*)	Precursory days for VLF amplitude enhancement in borehole
7.8	14
7.3	7
5.3	3
6.4	4
5.1	2

11 April 2015 in Figure 3 *a*, where it coincides with the enhancement in amplitude anomaly. However, the anomaly on this day is not due to lightning because, if it were so, such anomalies would have occurred on other days of lightning as well. This argument is also strengthened by the fact that on 11 April 2015, the number of lightning strokes occurred was 202 only, whereas on other days of lightning such as on 2 and 3 April and 19 May 2015, there were much higher strokes between 971 and 1663. Further, the possibility of only a few strokes occurring in VLF data will be eliminated on account of averaging the data for a longer time (10 h). In view of the above, it may be argued that anomalous amplitude enhancement observed in VLF data on 11 April 2015 may not be attributed to lightning activity.

Reports indicating that VLF data may be affected by solar–terrestrial phenomena like solar flares and solar eclipse are available[18]. Keeping this in view, we have examined the effects of these factors on the diurnal variation of the normalized electric field in Figure 3. Influence of these factors could not be seen on the diurnal variation on the anomalous days.

There are evidences that VLF data may also be affected by meteorological parameters like rainfall, wind speed, temperature and pressure of the atmosphere[19]. In view of these causative factors, first we looked for rainy days of April and May 2015 in which anomalous enhancements in VLF amplitudes were observed in our data, especially on 11 April and 5 May 2015. It was observed that there was no rainfall on the days in which these enhancements occurred. Thus, these enhancements may not be attributed to rainfall. Further, for examining the effect of wind speed, temperature and pressure of the atmosphere on amplitude of VLF data, daily variations of

these meteorological parameters for April and May 2015 were plotted and Figure 5 shows the results. It is clear from the figure that there is no significant variation in these parameters on the days on which VLF amplitude anomalies occurred (i.e. 11 April and 5 May 2015). Thus, the VLF amplitude anomalies observed on these days may not be due to these meteorological parameters.

The possibility of VLF data being affected by local building noises and power-line radiations and their harmonics may be ruled out on account of the use of differential amplifier and notch filter in the experimental set-up, consideration of night-time data for the analysis, and the antenna being underground in a PVC pipe. Moreover, VLF amplitude anomaly observed on 11 April and 5 May 2015 may not be due to instrumental errors because, if it were so, erroneous data would have appeared on other days of observations as well.

Theoretical modelling for confirmation of source

In order to explain how electromagnetic radiations were generated in the preparation zones of these earthquakes and their aftershocks and reached the Mathura observatory and caused the amplitude enhancements seen on 11 April and 5 May 2015, we have developed a theoretical model. A detailed description of the model is presented below.

Microcracks are generated as a result of the phenomenon of microfracturing which comes into play when growing stresses on the basement rocks reach the yield point[20]. When these microcracks propagate through a material, strain energy stored in the preparation zone is released through them. During the opening of cracks, charges of opposite polarity are developed on the newly formed crack surfaces either due to surface electrification or contact electrification, or both[21]. These opening cracks during their propagation behave like radiating dipoles (due to change in length and charge on their surfaces) and hence emit electromagnetic radiations[22]. The magnitude of electric field radiated due to a radiating dipole in a field point located at a distance r ($> r_c$) from it is given by the following equation[23]

$$E_r = \frac{\mu_0 \mu_r \varepsilon^2 p_0}{4\pi r}, \tag{1}$$

where μ_0, μ_r, ω and p_0 are permeability of free space, relative permeability, angular frequency of wave radiated from dipole and dipole moment of electric dipole respectively. Here, r_c is the critical distance of the field point from the radiating dipole beyond which static and conductive electric fields produced by the dipoles vanish and only the radiating field exists. It is expressed as[24]

$$r_c = \frac{|F(\omega)|^{1/2}}{\omega\sqrt{\mu\varepsilon}},$$

where

$$|F(\omega)| = \frac{i\omega}{i\omega + \frac{1}{\tau}} \text{ and } \tau = \frac{\varepsilon}{\sigma}$$

is the time constant. For the signal of frequency 3.012 kHz, its value is 16 km.

Reduction in strength of electric field (E_r) of radiating dipole when it propagates in the crustal region is governed by the relation

$$E_s = E_r e^{-\alpha r}, \tag{2}$$

where α is the attenuation constant for ground and E_s is its strength at the earth's surface.

Substituting the value of E_r from eq. (1) in eq. (2), we get

$$E_s = \left(\frac{\mu_0 \mu_r \omega^2 p_0}{4\pi r}\right) e^{-\alpha r}. \tag{3}$$

In the crustal region non-ferromagnetic materials are abundant and hence $\mu_r = 1$. Thus, eq. (3) reduces to

$$E_s = \left(\frac{\mu_0 p_0 \omega^2}{4\pi r}\right) e^{-\alpha r}. \tag{4}$$

After originating from the source (i.e. focal region, depth = 8.22 km), the wave electric field first reaches the earth's surface within certain range of distances (≈21–27 km) and then propagates through the atmosphere and suffers attenuation again in it, and finally reaches the observing station at a distance r' (distance between points of emanation and reception of electromagnetic waves both lying on the earth's surface). This attenuation of wave field in the atmosphere is expressed as

$$E_0 = E_s e^{-\alpha' r'}, \tag{5}$$

where α' is the attenuation constant of air.

Substituting the value of E_s from eq. (4) in eq. (5), we have

$$E_0 = \left(\frac{\mu_0 p_0 \omega^2}{4\pi r}\right) e^{-\alpha r} e^{-\alpha' r'} = \left(\frac{\mu_0 p_0 \omega^2}{4\pi r}\right) e^{-(\alpha r + \alpha' r')}. \tag{6}$$

Attenuation constants for ground and air are governed by the relations[25]

$$\alpha = \omega\sqrt{\frac{\mu\varepsilon}{2}}\left[\sqrt{1 + \left(\frac{\sigma_g}{\varepsilon\omega}\right)^2} - 1\right]^{1/2}. \tag{7}$$

$$\alpha' = \frac{\sigma_a}{2}\sqrt{\frac{\mu_0}{\varepsilon_0}} \text{ (for VLF waves, at } \sigma_g = 10^{-5} \text{ S/m)}, \quad (8)$$

where μ is the permeability of ground, ε the permittivity of ground, ε_0 the permittivity of free space or air, σ_g the conductivity of ground and σ_a is the conductivity of free space or air.

Substituting the values of α and α' from eqs (7) and (8) in eq. (6), we get

$$E_0 = \left(\frac{\mu_0 p_0 \omega^2}{4\pi r}\right) e^{-\left[\frac{\sigma_a}{2}\sqrt{\frac{\mu_0}{\varepsilon_0}}r' + \left\{\omega\sqrt{\frac{\mu\varepsilon}{2}}\left[\sqrt{1+\left(\frac{\sigma_g}{\varepsilon\omega}\right)^2}-1\right]^{1/2}\right\}r\right]}. \quad (9)$$

This is the expression for the strength of electric field radiated by a dipole when it is assumed to be present in the preparation zone of an impending earthquake. Similar dipoles are generated in the strained zone on account of accumulating stresses which are randomly oriented and distributed in space and time. An ensemble of N such dipoles (each of dipole moment p_0) exists in the preparation zone of an earthquake which is equivalent to a single dipole of moment P. Due to very small size and extremely low charge on dipoles their dipole moment is very less ($p_0 \approx 10^{-14}$ Coul × m) (ref. 26) and hence interaction in them can be neglected[25], i.e. $\sum p_i p_j = 0$.

$$P^2 = (\sum p_i)^2 = (\sum p_i^2 + 2\sum p_i p_j) = \sum p_i^2 = N p_0^2,$$

$$P = N^{1/2} p_0. \quad (10)$$

Thus, from eqs (9) and (10), net electric field produced by the ensemble of radiators is given by

$$E_{\text{net}} = \left(\frac{\mu_0 N^{1/2} p_0 \omega^2}{4\pi r}\right) e^{-\left[\frac{\sigma_a}{2}\sqrt{\frac{\mu_0}{\varepsilon_0}}r' + \left\{\omega\sqrt{\frac{\mu\varepsilon}{2}}\left[\sqrt{1+\left(\frac{\sigma_g}{\varepsilon\omega}\right)^2}-1\right]^{1/2}\right\}r\right]}. \quad (11)$$

The value of N can be estimated as follows

$$N = V \times n. \quad (12)$$

In eq. (12), n is the limiting value of crack density which is obtained from the expression[27]

$$n = \frac{1}{l^3}, \quad (13)$$

where l is the crack length. In eq. (12), V is the volume of the strained zone which can be obtained by the following relation given by Khattri *et al.*[28]

$$V = \frac{9}{8}\pi A^{3/2}. \quad (14)$$

Here A is the dislocation/rupture area which can be computed using the Wyss relation[29]

$$M = \log A + 4.15, \quad (15)$$

where M is the magnitude of the earthquake as measured from surface waves. Equation (15) is valid for $M > 5.6$.

Putting the value of V and n from eqs (13) and (14) in eq. (12), we get

$$N = \frac{\frac{9}{8}\pi A^{3/2}}{l^3} \quad (16)$$

For the Nepal earthquakes of magnitude $M = 7.8$ and 7.3 (measured from seismic moment), the dislocation/rupture area was found to be 8.9×10^9 and 2.8×10^9 m^2 respectively, while for their aftershocks of magnitude $M = 6.1$, 6.6 and 6.3 it was 1.8×10^8, 5.6×10^8 and 2.8×10^8 m^2 respectively, using eq. (15) given by Wyss[29].

Substituting the value of N from eq. (16) to eq. (11) we have

$$E_{\text{net}} = \left(\frac{\mu_0 p_0 \omega^2}{4\pi r}\right) \times \left(\frac{\frac{9}{8}\pi A^{3/2}}{l^3}\right)^{1/2} \times e^{-\left[\frac{\sigma_a}{2}\sqrt{\frac{\mu_0}{\varepsilon_0}}r' + \left\{\omega\sqrt{\frac{\mu\varepsilon}{2}}\left[\sqrt{1+\left(\frac{\sigma_g}{\varepsilon\omega}\right)^2}-1\right]^{1/2}\right\}r\right]}. \quad (17)$$

Equation (17) gives the required expression for the net electric field produced by the ensemble of elementary radiators existing in the preparation zone of an impending earthquake.

Finally, for confirming the observed amplitude enhancements from the model presented earlier, the strength of electric field at the field point (observing station, Mathura) due to the presence of radiators in the preparation zone of the Nepal earthquakes was calculated considering the following values of various parameters: $p_0 = 10^{-14}$ Coul × m (ref. 26), $\sigma_g = 10^{-5}$ S/m (ref. 30), $\sigma_a = 10^{-14}$ S/m (ref. 31), $l = 10^{-3}$ m (ref. 27), $\mu_0 = 4\pi \times 10^{-7}$ F/m, $\varepsilon_0 = 8.85 \times 10^{-12}$ C^2/Nm^2, $r' = 672.43$, 805.65, 687.41, 749.97, 819.95 km, $\mu = \mu_0$ and $\varepsilon = 10\varepsilon_0$ (for the crustal region), $\omega = 2\pi f = 2 \times 3.14 \times 3.012 \times 10^3$, $A = 8.9 \times 10^9$ m^2, 2.8×10^9 m^2, 1.8×10^8 m^2, 5.6×10^8 m^2, 2.8×10^8 m^2.

It is worthwhile to mention here that we have considered those r values (beyond critical distance r_c) from the focal points of Nepal earthquakes and their aftershocks to points on the earth's surface from where significantly strength of electric field would leak in the atmosphere which reaches the observing station through atmosphere suffering refraction at each layer of the atmosphere, and interact with the antenna leading to amplitude enhancements

at the observing site. However, the signals emanating from other places (i.e. other values of r and hence r') would reach the regions lying before or beyond the observing station Mathura.

Figure 6 is a schematic diagram showing different parameters, epicentre, atmospheric layers, whole process of electromagnetic wave propagation from earthquake focus (in the preparation zone) to the earth's surface, and then finally to the observing station Mathura through the atmosphere.

On substituting these values of different parameters in eq. (17), the strength of electric fields due to equivalent radiator lying in the preparation zones of the two Nepal earthquakes and their aftershocks at the observing station Mathura was $\approx 4.8 \times 10^{-9}$ and $\approx 2.7 \times 10^{-9}$ V/m respectively. These fields interacted with the antenna of length 120 m and caused a voltage in the order of 5.7×10^{-7} and 3.25×10^{-7} V in the borehole antenna on 11 April and 5 May 2015 respectively. It is noteworthy to mention here that the estimations carried out for voltage induced on the antenna are correct up to a certain limit. However, some minor variation in these values may be due to variation in the values of modelling parameters. Further, sensitivity analysis should be carried out with different parameters, which is not done in our case. These voltages were amplified by the antenna set-up. (Gain $\approx 1.28 \times 10^5$. A known input signal was fed at the input terminals of the antenna set-up and then voltage at its output terminals was measured. Finally, using the relation gain = output/input its gain was computed.) Hence their values were increased to 73.13 and 41.55 mV between its output terminals on 11 April and 5 May 2015, which are close to average values of the night-time VLF data as observed on these days in borehole antenna at Mathura observatory located about 700–800 km from the focal regions of Nepal earthquakes and their aftershocks. The values of recorded output voltages (i.e. 73.13 and 41.55 mV) were obtained by multiplying the gain of antenna (1.28×10^5) with voltage induced at its input terminals (i.e. 5.7×10^{-7} and 3.25×10^{-7} V). Thus, our theoretical model supports the experimental results obtained at Mathura observing station in case of the Nepal earthquakes and their aftershocks. Amplitude anomalies at such long distances have also been reported in the literature[4,32]. It is worthwhile to mention here that we have assumed that electromagnetic signals emanating from the radiating dipoles existing in preparation zones of the Nepal earthquakes and their aftershocks first propagated through the crustal region and reached the earth's surface, and then from there to the observing station through the atmosphere. Similar mechanism for the propagation of seismogenic emissions has also been suggested by other workers[25].

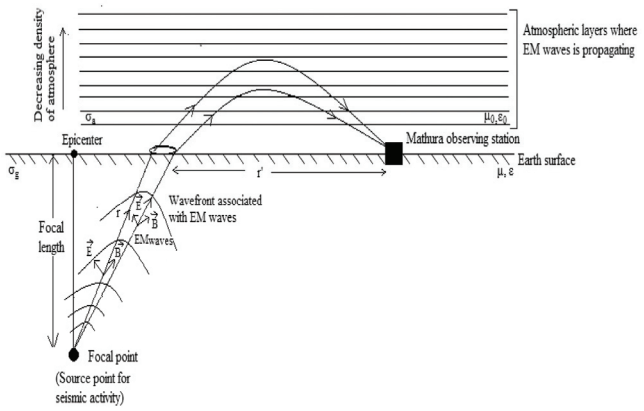

Figure 6. Schematic diagram showing the whole process of transmission of electromagnetic radiations from focus of the earthquake to the earth surface and then to the observing site through the atmosphere.

Discussion and conclusion

From the results presented above, it is clear that anomalous VLF amplitude enhancements observed in the borehole on 11 April and 5 May 2015 are not correlated with any of the factors due to solar–terrestrial disturbances or meteorological parameters, except those of the Nepal earthquakes and their aftershocks. The theoretical modelling of generation and wave propagation yielding almost the same values of electric field as observed experimentally at the Mathura station confirms the sources of the anomalies in the Nepal earthquakes.

Statistical analysis of daily variations of amplitude of vertical components of subsurface VLF electric field changes for January to July 2015 using the mean and standard deviation approach was carried out for two major earthquakes of magnitude $M = 7.8$ and $M = 7.3$ and their aftershocks that occurred on 25 April and 12 May 2015 in Khudi and Kodari regions of Nepal respectively. Significant enhancements in the normalized amplitude of daily variations of VLF data were observed 7-days before the occurrence of these earthquakes and their aftershocks. This result is in good agreement with the findings of earlier workers[33,34]. Further, these amplitude enhancements have been examined in light of other non-seismic sources such as solar–terrestrial disturbances, lightning and meteorological parameters such as wind speed, temperature and pressure of the atmosphere. It was found that anomalous VLF amplitude enhancements are not related to these sources. In addition, we have developed a model for the generation and propagation mechanisms of seismogenic emissions recorded at the observing station Mathura corresponding to the said earthquakes, assuming an ensemble of elementary radiators randomly oriented and distributed in space and time in the preparation zones of these earthquakes and their aftershocks. The calculation of electric field using this model results in the same values as observed experimentally using the borehole antenna.

1. Gokhberg, M. B., Morgunov, V. A., Yoshino, T. and Tomizawa, I., Experimental measurement of electromagnetic emissions possibly

related to earthquakes in Japan. *J. Geophys. Res*., 1982, **87**(B9), 7824–7828.
2. Hattori, K., Han, P., Yoshino, T., Febriani, F., Yamaguchi, H. and Chen, C. H., Investigation of ULF Seismo-magnetic phenomena in Kanto, Japan during 2000–2010: Case studies and statistical studies. *Surv. Geophys*., 2013, **34**(3), 293–316.
3. Fujinawa, Y., Noda, Y., Takahashi, K., Kobayashi, M., Takamatsu, K. and Natsumeda, J., Field detection of microcracks to define the nucleation stage of earthquake occurrence. *Int. J. Geophys*., 2013, **2013**(7), 1–18.
4. Singh, R. P., Singh, B., Mishra, P. K. and Hayakawa, M., On the Lithosphere-atmosphere coupling of seismo-electromagnetic signals. *Radio Sci*., 2003, **38**(4), 1–10.
5. Pundhir, D., Singh, B. and Singh, O. P., Anomalous TEC variations associated with the strong Pakistan–Iran border region earthquake of 16 April 2013 at a low latitude station Agra, India. *Adv. Space Res*., 2014, **53**(2), 226–232.
6. Frid, V., Rabinovitch, A. and Bahat, D., Fracture induced electromagnetic radiation. *J. Phys. D. Appl. Phys*., 2003, **36**(13), 1620–1628.
7. Hayakawa, M., *Earthquake Prediction with Radio Techniques*, John Wiley and Sons, Singapore, 2015.
8. Pulinets, S. and Ouzounov, D., *The Possibility of Earthquake forecasting: Learning from Nature*, IOP Publishing, Bristol, 2018.
9. Qian, S., Yian, J., Cao, H., Shi, S., Lu, Z., Li, J. and Ren, K., Results of observations on seismo-electromagnetic waves at two earthquake experimental areas in China. In *Electromagnetic Phenomena Related to Earthquake Prediction* (eds Hayakawa, M. and Fujinawa, Y.), Terra. Sci. Pub. Co Tokyo, 1994, pp. 205–211.
10. Fujinawa, Y. and Takahashi, K., *Electromagnetic Radiations at the Time of the Great Kurile Island Earthquake of 1994*, In IUGG Meeting 1995, Boulder, Colorado, 1995.
11. Singh, R. P. and Singh, B., Detection and identification of VLF seismo-electromagnetic signals. *Curr. Sci*., 2000, **78**(4), 492–498.
12. Maurya, A. K., Venkatesham, K., Tiwari, P., Vijaykumar, K., Singh, R., Singh, A. K. and Ramesh, D. S., The 25 April 2015 Nepal Earthquake: Investigation of precursor in VLF subionospheric signal. *J. Geophys. Res. Space Phys.*, 2016, **121**(10), 403–416.
13. Muto, F., Kasahara, Y., Hobara, Y., Hayakawa, M., Rozhnoi, A., Solovieva, M. and Molchanov, O. A., Further study on the role of atmospheric gravity waves on the seismo ionospheric perturbations as detected by subionospheric VLF/LF propagation. *Nat. Hazards Earth Syst. Sci*., 2009, **9**, 1111–1118.
14. Molchanov, O. A. and Hayakawa, M., Subionospheric VLF signal perturbation possibly related to earthquakes. *J. Geophys. Res*., 1998, **103**(A8), 17489–17504.
15. Pundhir, D., Singh, B., Lakshmi, D. R. and Reddy, B. M., A study of ionospheric precursors associated with the major earthquakes occurred in Pakistan region. *J. Ind. Geophys. Union*, 2015, **19**(1), 71–76.
16. Rikitake, T., *Earthquake Prediction*, Elsevier, Amsterdam, 1976.
17. Choudhury, A., De, B. K., Guha, A. and Roy, R., Long-duration geomagnetic storm effects on the D region of the ionosphere: Some case studies using VLF signal. *J. Geophys. Res: Space Phys*., 2015, **120**(1), 778–787.
18. Selvakumaran, R. *et al.*, Solar flares induced D-region ionospheric and geomagnetic perturbations. *J. Atmos. Sol. Terr. Phys*., 2015, **123**, 102–112.
19. Rozhnoi, R., Solovieva, M., Levin, B., Hayakawa, M. and Fedun, V., Meteorological effects in the lower ionosphere as based on VLF/LF signal observations. *Nat. Hazards Earth Syst. Sci.*, 2014, **14**, 2671–2679.
20. Hadjicontis, V., Mavromatou, C. and Ninos, D., Stress induced polarization currents and electromagnetic emission from rocks and ionic crystals, accompanying their deformation. *Nat. Hazards Earth Syst. Sci*., 2004, **4**(5–6), 633–639.
21. Takeuchi, A. and Nagahama, H., Voltage changes induced by stick–slip of granites. *Geophys. Res. Lett*., 2001, **28**(17), 3365–3368.
22. Takeuchi, A. and Nagahama, H., Electric dipoles perpendicular to a stick–slip plane. *Phys. Earth Planet Int*., 2006, **155**(3), 208–218.
23. Tsarev, V. A. and Sasaki, H., Low frequency seismogenic electromagnetic radiation: how does it propagate in the earth's crust and where it can be detected? In *Atmospheric and Ionsopheric Electromagnetic Phenomena Associated with Earthquakes* (ed. Hayakawa, M.), Terra Sci. Pub. Co., Tokyo, 1999, pp. 383–393.
24. Yoshida, S. and Ogawa, T., Electromagnetic emissions from dry and wet granite associated with acoustic emissions. *J. Geophys. Res*., *Solid Earth*, 2004, **109**(B9), 1–11.
25. Ikeya, M., Kinoshita, Y., Matsumoto, H., Takaki, S. and Yamanaka, C., A model experiment for electromagnetic wave propagation over long distances using waveguide terminology. *Jpn. J. Appl. Phys*., 1997, **36**(11B), L1558–L1561.
26. Ogawa, T., Oike, K. and Miura, T., Electromagnetic radiations from rocks. *J. Geophys. Res.*, 1985, **90**(D4), 6245–6249.
27. Surkov, V. V., ULF electromagnetic perturbations resulting from the fracture and dilatancy in the earthquake preparation zone. In *Atmospheric and Ionospheric Electromagnetic Phenomena Associated with Earthquakes* (ed. Hayakawa, M.), Terra Sci. Pub. Co., Tokyo, 1999, pp. 371–382.
28. Khattri, K. N., On the estimation of volume of strain in earthquakes. *Pure Appl. Geophys*., 1971, **87**(1), 38–42.
29. Wyss, M., Estimating maximum expectable magnitudes of earthquakes from fault dimensions. *Geology*, 1979, **7**, 336–340.
30. Bortnik, J., Bleier, T. E., Dunson, C. and Freund, F., Estimating the seismotelluric current required for observable electromagnetic ground signals. *Ann. Geophys*., 2010, **28**(8), 1615–1624.
31. Rycroft, M. J., Harrison, R. G., Nicoll, K. A. and Mareev, E. A., An overview of earth's global electric circuit and atmospheric conductivity. *Space Sci. Rev*., 2008, **137**(1–4), 83–105.
32. Fujinawa, Y. and Takahashi, K., Electromagnetic radiations associated with major earthquakes. *Phys. Earth Planet. Int*., 1998, **105**(3–4), 249–259.
33. Uyeda, S., Nagao, T., Orikara, Y., Yamaguchi, T. and Takahashi, I., Geoelectric potential changes: Possible precursors to earthquake in Japan. *Proc. Natl. Acad. Sci. USA*, 2000, **97**(9), 4561–4566.
34. Singh, R. P., Kumar, M., Singh, O. P. and Singh, B., Subsurface VLF electric field emissions associated with regional earthquakes. *Ind. J. Radio Space Phys*., 2009, **38**, 220–226.

ACKNOWLEDGEMENTS. We thank the Ministry of Earth Sciences, Government of India, for providing funds through a major research project. Thanks are also due to World Data Center for Geomagnetism for providing magnetic storms data, United States Geological Survey for furnishing the earthquake data, National Aeronautics and Space Administration (NASA) for providing solar eclipse data, National Oceanic and Atmospheric Administration (NOAA) for furnishing the data related to meteorological parameters, through their websites respectively.

Received 31 March 2020; revised accepted 6 April 2021

doi: 10.18520/cs/v121/i4/551-559